Laser heating of cantilevered tips: Implications for photoinduced force microscopy

Bongsu Kim and Eric O. Potma

Phys. Rev. B **100**, 195416 — Published 18 November 2019

DOI: 10.1103/PhysRevB.100.195416

Laser heating of cantilevered tips: implications for photo-induced force microscopy

Bongsu Kim[1] and Eric O. Potma[1,*]

[1] *Department of Chemistry, University of California, Irvine, California 92697, USA*

(Dated: November 6, 2019)

Photo-induced force microscopy (PiFM) measures changes in the force between an atomically sharp tip and the sample under the influence of applied radiation. Several mechanisms contribute to the overall force, including forces introduced due to thermal heating of the sample and the tip. In this contribution we study the effect of laser heating of the retracted tip under illumination conditions relevant to PiFM and how it affects the mechanical resonance properties of the cantilever. Using a gold-coated silicon cantilever with its tip irradiated by a tightly focused 532 nm laser beam, we find that the tip temperature increases linearly at 7.5 K/mW of average laser power, irrespective of whether the laser is pulsed or continuous wave. The temperature rise gives rise to a decrease of the cantilever's spring constant and an increase of the damping coefficient. We demonstrate that for retracted tips, these thermally-induced changes to the mechanical resonance only moderately impact the measured photo-induced force, as the measured scattering force is at least an order of magnitude stronger than the effective force introduced by laser heating under experimentally relevant conditions.

I. INTRODUCTION

Photo-induced force microscopy (PiFM) is a nanospectroscopic imaging technique which measures the electromagnetic force exerted by the optical field on an atomically sharp tip. The PiFM approach has been used to map optical fields confined to the nanoscale[1–4], as well as to map forces between induced dipoles in the tip and the sample through the gradient force, thus allowing spectroscopic contrast[5]. In spectroscopic mode, PiFM proved capable of visualizing molecular samples based on linear electronic[6,7] and vibrational absorption[8], as well as excited state absorption[9] and vibrational transitions driven by stimulated Raman scattering[10].

Although the PiFM technique aims to probe the mutual electromagnetic force between the induced polarization densities in the tip and in the sample (induced dipole force), thermal heating near the tip/sample junction may introduce additional effects that can sometimes dominate the measurement. Energy contained in the light field is inevitably absorbed by both the tip and sample materials, producing a local rise in temperature and a subsequent expansion of the materials. Expansion-related forces have been suggested to constitute a significant contribution to PiFM measurements, especially in mid-infrared absorption measurements where the gradient force has been predicted to be weaker than expansion forces[11,12]. Several scan probe techniques, including photothermal-induced resonance microscopy (PTIR)[13,14] and peak force infrared microscopy (PFIR)[15], make use of thermal expansion to probe molecular absorption at the nanoscale. Beyond measuring sample expansion directly, photo-induced force measurements are also sensitive to the gradient of the (attractive) thermally modulated interaction force, which can dominate the PiFM signal even in non-contact mode[16]. Other work has specifically focused on laser heating of the tip, and how the resulting thermal radiation emanating from the tip's apex can be used for near-field microscopy in the thermal infrared range[17].

In this work, we study the effect of tip heating in PiFM. In order to discriminate the effects of sample heating from heating of the tip-cantilever system, we focus here on the limit of large tip/sample distances, implying that the effect of sample expansion and tip/sample interactions can be excluded. This limit allows us to study how heating of the tip affects the mechanical properties of the cantilever and how the thermally induced changes in turn affect the measurement of the photo-induced scattering force. Whereas previous work has focused on laser heating of the tip to several hundreds of degrees Celsius[18], here we are interested in the limit of low laser powers (~ 1 mW or less) that are relevant to PiFM. In Section II, we develop a model for the measured photo-induced force in the presence of thermally induced changes to the cantilever's spring constant and damping coefficient. In Section III, we simulate the heat transfer in the tip-cantilever system and study how it affects the resonance properties of the cantilever beam. We perform measurements of the cantilever's resonance frequency and quality factor under the influence of laser heating at the tip in Section IV, and connect these measurements to the simulations to obtain an estimate of the tip temperature. Lastly, in Section V, we determine the effect of laser heating and thermal gradients in the cantilever on the measurement of the scattering force.

II. PHOTO-INDUCED FORCES PROBED BY HEATED TIPS

In this Section, we consider a simple analytical model for describing the effect of laser heating of the tip-cantilever system on photo-induced force microscopy experiments. Our goal is to find an expression for the measured optical force that includes the impacts of thermal heating of the oscillating cantilever beam.

We first consider the cantilever dynamics in the presence of an optical force, where we allow the beam parameters to change due to thermal loading by the laser beam. The cantilever motion can be modeled as a sinusoidally driven damped oscillation along a generalized coordinate ε, which is aligned along the z-direction and describes the time-dependent displacement of the tip. The displacement ε_i contributed by a given eigenmode i is described by:

$$m\ddot{\varepsilon_i} + (b_i + \Delta b_i)\dot{\varepsilon_i} + (k_i + \Delta k_i)\varepsilon_i = F_d^i \cos\omega_d t + F_{\rm opt}^i(z,t) \quad (1)$$

where m is the effective mass of the cantilever, k_i and b_i are the spring constant and damping coefficient of the i-th eigenmode, respectively. Δk_i and Δb_i represent the change of the spring constant and damping coefficient of the i-th eigenmode due to laser heating. F_d^i and ω_d are the mechanical driving force acting on mode i and the angular frequency of the mechanically driven motion. $F_{\rm opt}^i$ represents the contribution of the photo-induced force $F_{\rm opt}$ acting on mode i. The optical force depends on the tip-sample distance z. In the long distance limit, we only need to consider the interaction between light and tip in Eq. 1, while the interactions between the tip and the sample surface, which include the van der Waals forces[19], hydration forces[20], and gradient forces[21], can be ignored. In the PiFM experiment, the laser illumination is modulated as a square wave by an acoustic optic modulator (AOM), which produces a periodically varying optical force $F_{\rm opt}$ that can be described as:

$$F_{\rm opt}(z,t) = F_{\rm opt}(z)\left[\frac{1}{2} + \frac{2}{\pi}\sum_{n=\rm odd}\frac{\sin(n\omega_m t)}{n}\right] \quad (2)$$

where ω_m is the laser modulation frequency. $F_{\rm opt}(z)$ can be expanded into a Taylor series as follows:

$$F_{\rm opt}(z) \approx F_{\rm opt}(z_0) + \frac{\partial F_{\rm opt}(z)}{\partial z}\Big|_{z_0}(z - z_0) + \cdots . \quad (3)$$

Due to the modulated light intensity, the thermal loading is also modulated, which implies that Δk_i and Δb_i are, in principle, time-varying parameters as well. However, in this work, we will consider only the time-averaged effect of laser heating on the tip-cantilever system. Under these conditions, we may assume that Δk_i and Δb_i are constants for a given intensity of the laser beam.

In the PiFM experiment, the cantilever is mechanically driven by ω_d and optically modulated by ω_m. The cantilever response is enhanced when tuning the driving frequencies close to an eigen frequency of the cantilever, in particular the first (ω_{01}) and second eigen (angular) frequencies (ω_{02}) of the cantilever beam. Here we will consider the case that the cantilever dynamics is comprised of two oscillatory motions, one at ω_1, near the first eigen frequency, and one at ω_2, near the second eigen frequency. We may thus write:

$$\varepsilon \equiv \varepsilon_1 + \varepsilon_2 = A_1 \sin(\omega_1 t + \theta_1) + A_2 \sin(\omega_2 t + \theta_2) \quad (4)$$

where A_i is the amplitude and θ_i is the phase shift of the oscillation. Note that ω_1 and ω_2 are the frequencies driven near the eigen frequency, and are not required to be exact eigen frequencies. From here, we set $\omega_d = \omega_2$, i.e. the mechanical driving frequency is near the second eigen frequency of the cantilever. When ω_m is set to ω_1, the PiFM measurement is directly sensitive to the optical force. This configuration is called *direct mode* (or homodyne) detection[5]. On the other hand, if ω_m is set to $\omega_2 \pm \omega_1$, the measurement is sensitive to the gradient of the optical force, also known as *sideband mode* (or heterodyne) detection[22,23].

For direct mode detection, an identification of the terms at angular frequency ω_1 yields the following equation:

$$m\ddot{\varepsilon}_1 + b_1'\dot{\varepsilon}_1 + k_1'\varepsilon_1 = \frac{2F_{\rm opt}}{\pi}\sin(\omega_1 t) - \frac{k_{\rm opt}A_1}{2}\sin(\omega_1 t + \theta_1) \quad (5)$$

where $b_i' = b_i + \Delta b_i$, $k_i' = k_i + \Delta k_i$, and $k_{\rm opt} = -\partial F_{\rm opt}/\partial z$. Since $|k_{\rm opt}A_1| < 0.1$ pN in practical experiments, the last term on the right hand side of Eq. (5) can be safely ignored[22]. A similar operation yields an expression for the motion probed in the side band detection mode:

$$m\ddot{\varepsilon}_1 + b_1'\dot{\varepsilon}_1 + k_1'\varepsilon_1 = \frac{-k_{\rm opt}A_2}{\pi}\cos(\omega_1 t + \theta_2) \quad (6)$$

Here ε has been set to $(z - z_0)$. In this derivation, we neglected cross terms related to the motions at ω_1 and ω_2. For cantilevers, the second resonance frequency is about 6 times higher than the first resonance frequency, producing cross terms that are much smaller than the magnitude of the motion along the fundamental frequencies. The resulting equations (5) and (6) correspond to the well known equations of motion for a sinusoidally driven damped oscillator. The solution to this equation yields expressions for the oscillation amplitude $A_1(\omega_1)$ for both the direct and sideband detection modes:

$$A_1 = \frac{B}{\sqrt{m^2({\omega'}_{01}^2 - \omega_1^2)^2 + {b_1'}^2\omega_1^2}} \quad (7)$$

where ${\omega'}_{01}^2 = k_1'/m$, and $B = 2|F_{\rm opt}|/\pi$ for the direct mode and $B = |k_{\rm opt}|A_2/\pi$ for the sideband mode.

Equation (7) implicitly includes the effect of laser heating through k_1' and b_1', which depend on Δk_1 and Δb_1, respectively. These terms can be extracted from independent measurements of the frequency f_i and the quality factor Q_i of the mechanical resonance:

$$f_i = \frac{1}{2\pi}\sqrt{\frac{k_i + \Delta k_i}{m}}, \quad (8)$$

$$Q_i = \frac{k_i + \Delta k_i}{2\pi f_i(b_i + \Delta b_i)}. \quad (9)$$

Because Δk_i and Δb_i change with temperature, thermal loading of the tip/cantilever system will produce a frequency shift and a change in the quality factor of the resonance. By measuring these changes directly, Δk_i and Δb_i can be retrieved, and their effect on PiFM can be then determined through Eq. (7). We will employ this approach in Section IV.

However, while instructive, such independent measurements are not always practical during actual PiFM measurements. Therefore, it is helpful to use an alternative metric that can be directly retrieved from PiFM measurements. Since PiFM measurements are typically performed by recording the cantilever response in both ω_1 and ω_2 channels, we may use the A_2 amplitude variations to inform the measurement of A_1. By multiplying both sides of Eq. (1) with $\sin(\omega_2 t+\theta_2)$ or $\cos(\omega_2 t+\theta_2)$, respectively, and then integrating over an oscillation period, we obtain the following expressions for Δk_2 and Δb_2:

$$\Delta k_2 = \frac{F_d}{A_2}\sin\theta_2 - (k_2 - m\omega_2^2), \tag{10}$$

$$\Delta b_2 = \frac{F_d}{A_2\omega_2}\cos\theta_2 - b_2, \tag{11}$$

The changes in spring constant and damping of the second resonance can be related to the changes of the first resonance through $\Delta k_1 = \alpha\Delta k_2$ and $\Delta b_1 = \beta\Delta b_2$, where α and β are cantilever-specific scaling factors that need to be determined experimentally. In Section V, we will show that this linear relation between the physical parameters of the first and second mode is justified and that this approach also leads to an accurate estimation of the effects of laser heating of the tip.

Finally, once Δk_1 and Δb_1 are retrieved from the measurement, the effect of laser heating on the optically induced force can be studied. In the direct detection mode, $|F_{opt}|$ can be obtained through Eq. (7) as

$$\begin{aligned} |F_{\rm opt}|^2 = (\pi^2/4)(&A_1^2[m^2(\omega_{01}^2-\omega_1^2)^2 + b_1^2\omega_1^2] \\ &+ A_1^2(\Delta k_1^2 + \Delta b_1^2\omega_1^2) \\ &+ A_1^2[2\Delta k_1 m(\omega_{01}^2-\omega_1^2) + 2b_1\Delta b_1\omega_1^2]) \ , \end{aligned} \tag{12}$$

where $\omega_{01}^2 = k_1/m$. The first term in Eq.(12) is the same as Eq.(26) in Ref. (5) when $F_{\rm int}$ is ignored, i.e., the tip-sample interaction is not considered. We see that the first term on the right hand side of Eq. (12) corresponds to the square of the scattering force F_{scat}, while the second term is entirely related to laser heating effect. We can interpret the second term as the square of an effective force due to heating, i.e. $F_{\rm heat}$. The last term of Eq.(12) is a cross term that depends on both $F_{\rm scat}$ and $F_{\rm heat}$. In standard PiFM measurements, we expect that the measured force is dominated by $F_{\rm scat}$ in the absence of tip-sample interactions. One of the objectives of this work is to determine to what extent $F_{\rm heat}$-related contributions affect such measurements.

III. SIMILATION OF HEATED CANTILEVER

Before discussing experiments, we wish to obtain a quantitative prediction of the effects of tip heating on the mechanical resonances of the cantilever. For this reason, we perform finite element method (FEM) simulations of the tip/cantilever system under the condition of thermal loading at the illuminated tip apex.

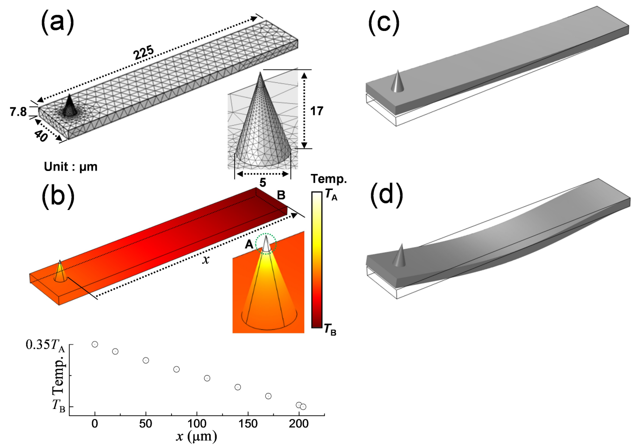

FIG. 1. FEM simulation of the tip/cantilever system in the presence of a thermal load. (a) Dimensions of the ACL type cantilever with tetrahedral blocks chosen as the finite elements. (b) Temperature distribution of cantilever in the stationary state. The surface temperatures of **A** and **B** are fixed and form the boundary conditions in the simulation. The inset graph shows the temperature gradient in the cantilever beam. (c) Simulated first and (d) second eigen modes of the cantilever.

The cantilever motions and eigenfrequencies are simulated with three-dimensional FEM using the COMSOL MULTIPHYSICS 5.0 software package, utilizing the Structural Mechanics and Heat Transfer modules. The relevant geometry is depicted in Figure 1(a), which is based on an ACL type cantilever. The dimensions of the cantilever are based on the cantilever used in the experiments (Section IV). The simulation is carried out in two steps. In the first step, the stationary state temperature distribution of the cantilever is calculated using heat transfer simulations in the Heat Transer module. In the simulation, the temperature is fixed at the end of the tip (**A** in figure 1 (b)) and at cantilever body (**B** in Figure 1(b)). The surface of the white cone **A** is set at a fixed value, ranging between 300.0 K to 420.0 K, for each simulation. Surface **B**, which is connected to the much larger body of the scan head, is fixed at room temperature (300.0 K). Note that the effect of heat loss into the surrounding medium (air) is assumed to be small and has been ignored in the present simulations.

As an initial condition, the body of the cantilever is set to 300.0 K. Simulations are then run with three kinds of diameters (D = 0.6, 0.8 and 1.0 μm, see also Fig. 2) for the base of the cone **A**. These diameters correspond to the spatial extent over which the focused laser spot couples to the tip apex. The Heat Transfer module uses the heat diffusion equation

$$\rho C_p \frac{\partial T}{\partial t} - \nabla \cdot (k \nabla T) = \Theta \tag{13}$$

where ρ, C_p, T, t, k and Θ are the density, heat capacity, temperature, evolution time, thermal conductivity and heat source in the cantilever body, respectively. In the simulation, we only consider the temperature distribution of the fully equilibrated, stationary state, implying that the time dependence of the temperature disappears ($\partial T/\partial t = 0$) in Eq. 13. In addition, there is no heat source in the cantilever body ($\Theta = 0$). Therefore, the stationary state should satisfy the Laplace equation ($\nabla^2 T = 0$), which is independent of the heat capacity and thermal conductivity. Figure 1(b) shows the temperature distribution of the cantilever in the stationary state.

In the second step, the eigen frequencies of the cantilever are found using the Solid Mechanics module. We use the temperature dependent physical properties for silicon, namely the density[24], the Young's modulus[25] and the thermal expansion coefficient[26]. A Poisson's ratio of the value 0.22 is used[27]. In the region or interest, the Poisson's ratio is found to change by less than 1 % due to temperature changes[28].

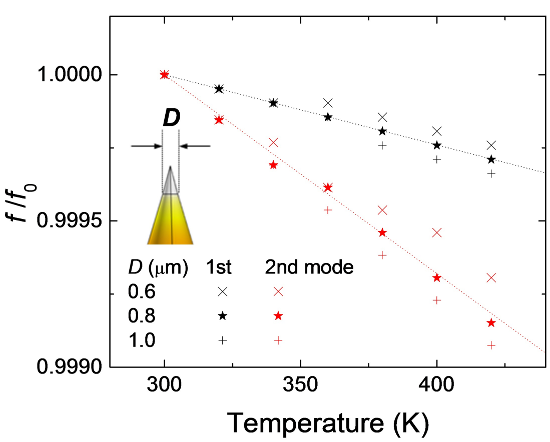

FIG. 2. Simulation of the relative resonance frequencies of the first and second eigen mode of the tip/cantilever system as a function the tip temperature. Cantilever dimensions are based on the cantilever used in the experiments. Results are shown for different diameters D of the base of the apex cone.

Figure 2 shows the relative shift of the resonance frequency as the temperature at the tip apex is increased. It is observed that both the first and second eigen frequencies decrease linearly with temperature, with a more rapid decrease for the second mode. Below 350 K, the simulations show that the variation with radius D is relatively minor. The simulation results can be be fitted with the following equation:

$$\frac{f}{f_0} = C(T - 300) + 1 \tag{14}$$

where C is a constant. The fit yields values $C = 2.4\ \mu\mathrm{K}^{-1}$ and $C = 6.8\ \mu\mathrm{K}^{-1}$ for the first and second mode, respectively. We will use the relation between temperature and frequency shift in Section IV to estimate the temperature of the tip apex during laser illumination experiments. We note that the although addition of a 40 nm gold layer to the cantilever beam reduces the absolute resonance frequencies of both the first and second mechanical resonances by as much as 3%, it does not affect the temperature dependence of the relative frequency shift displayed in Figure 2 within the accuracy of the simulation.

IV. RESONANCE FREQUENCY SHIFT

In this Section, we experimentally measure the cantilever resonance properties under the condition that the tip is illuminated with a focused laser beam. For these measurements, we use either a continuous wave (cw) laser (Crystalase) at $\lambda = 532$ nm or a pulsed laser tuned to a center wavelength of 532 nm. The pulsed light source consists of a Ti:sapphire-pumped optical parametric oscillator (Inspire OPO, Radiantis), delivering 200 fs pulses at 80 MHz. The beam is modulated by an acoustic optic modulator at frequency f_m. The modulated laser beam is directed to a scan probe microscope (Vistascope, Molecular Vista), which includes an objective lens (NA = 0.95, Olympus) mounted in an inverted microscope configuration. The laser beam is focused onto a borosilicate glass slide (0.17 mm thickness), and the tip of a gold-coated silicon cantilever (ACLGG, Applied NanoStructures) is placed in the laser focus. The cantilever used in the experiments has its first (f_{01}) and second (f_{02}) resonance frequencies at 149 kHz and 922 kHz, respectively. The quality factors are 393 and 554 for the first and second resonance, respectively. The measurements are performed under ambient conditions.

We are first interested in characterizing the spatial extent over which the light interacts with the tip apex. For this purpose, we perform PiFM measurements by keeping the focused laser beam fixed in space and scanning the tip laterally across the focal spot. In these measurements, the PiFM signal is detected in the sideband mode, with f_m tuned to $f_{01} + f_{02}$[22]. The cantilever is demodulated at f_{01} for detecting the PiFM signal while it is mechanically driven at f_{02} for AFM feedback. For the tapping mode measurements, the average tip-substrate distance is set to 15 nm with an oscillation amplitude of 13 nm.

Figures 3(a) and (b) show the measured spot sizes for the focused cw and pulsed laser beams, respectively. Panels 3(c) and (d) depict the corresponding one-dimensional cross sections. Using a Gaussian fit, we find full-width half maximum diameters of 0.710 μm and 0.885 μm for

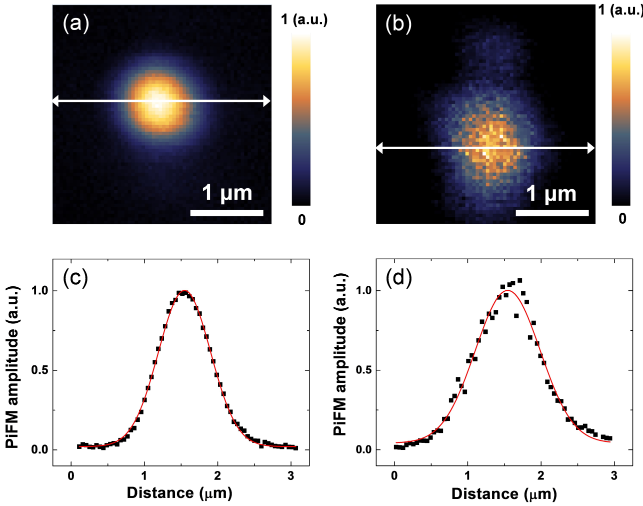

FIG. 3. Spot size measurement in PiFM when the tip is illuminated by (a) cw laser, and (b) pulsed laser. White arrows in each panel show the position where cross sections are taken, displayed in (c) and (d).

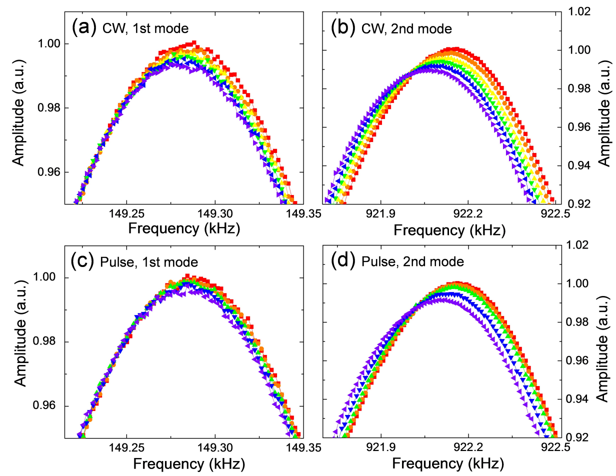

FIG. 4. Resonance curves as a function of average laser power. (a) First and (b) second eigen mode of the cantilever while illuminated by the cw laser. Laser powers in focus are 0.00 mW (red squares), 0.32 mW (orange circles), 0.63 mW (yellow triangles), 0.95 mW (green triangles), 1.26 mW (blue triangles) and 1.58 mW (purple triangles). (c) First and (d) second eigen mode of the cantilever while illuminated by the pulsed laser. Laser powers in focus are 0.00 mW (red squares), 0.18 mW (orange circles), 0.35 mW (green triangles), 0.70 mW (blue triangles) and 1.12 mW (purple triangles).

the CW and pulsed laser spots, respectively. The observed differences between the cw and pulsed modes are due mainly to the beam quality rather than the temporal nature of the photon flux. We will use the measured diameters as estimates for the diameter D used in the simulations.

We next focus on the changes to the mechanical resonance properties of the tip/cantilever system as the light is coupled to the tip at various average laser powers. For these measurements, the tip is placed in the center of the focal spot, at a distance of 70 nm from the glass slide. Under these conditions, we record the resonance curve by sweeping the driving frequency through the cantilever resonance. Figure 4 presents the relative resonance curve shift of the first and second eigen mode of the cantilever, measured in both the cw and pulsed illumination modes. The general trend observed from the measurements is that the mechanical resonance shifts toward lower frequencies as the laser power is increased, both for the first and the second eigen mode, in either cw or pulsed illumination.

From these measurements, it is possible to extract the resonance frequencies and quality factors by fitting the resonance curves with the spectral response function of a sinusoidally driven damped oscillator. The results of the fitting procedure are shown in Figure 5. Panel 5(a) shows the relative frequency shift f/f_0 of the resonance, where f_0 is the resonance frequency in the absence of the laser beam, as a function of the average laser power. Both the first (black) and second (red) eigen modes show a linear decrease with increasing laser power, corroborating the trend observed in the simulations. Again, the differences between measurements using cw (solid symbols) or pulsed (open symbols) laser illumination are relatively small, underlining that the interaction between the light field and the tip is governed by the average intensity and not by the peak intensities. Energy exchange between the light field and the material raises the temperature of the material, changing the physical properties of the cantilever, including the density[24], the Young's modulus[25], the Poisson's ratio[28], and the thermal expansion coefficient[26]. The lowering of the resonance frequency can be attributed to the softening of the material as the temperature is raised[18,29,30]. In addition, a rise in temperature and a temperature gradient in the material also leads to a decrease in the Q-factor[31–33]. The extracted change in the quality factor (Q/Q_0) is shown in Panel 5(b), revealing the expected linear decrease with laser power for both eigenmodes of the cantilever.

Using Eqs. 8 and 9, the changes in the spring constant Δk_i and damping coefficient Δb_i can be extracted from the measured frequency shift and quality factor. The results are shown in panels 5(c) and (d). We observe that the spring constant linearly decreases with laser power for both the first and second eigen modes of the cantilever, shown in panel 5(c), although the change is more significant for the second mode. We find that ratio between the change Δk_1 in the first and second mode for this cantilever is constant at $\Delta k_1/\Delta k_2 = \alpha = 8.8527 \times 10^{-3}$. The change in the damping coefficient, on the other hand, grows with incident laser power, as depicted in panel 5(d). Again, the slope of the second eigen mode is much steeper than for the first eigen mode in Figure 5(d), yet the ratio $\Delta b_1/\Delta b_2$ is constant for all laser powers examined. We find that $\Delta b_1/\Delta b_2 = \beta = 5.8835 \times 10^{-2}$ for the cantilever used in these experiments. In Section V, we will use the values of α and β to extract information about Δk_1 and Δk_2 directly from PiFM measurements.

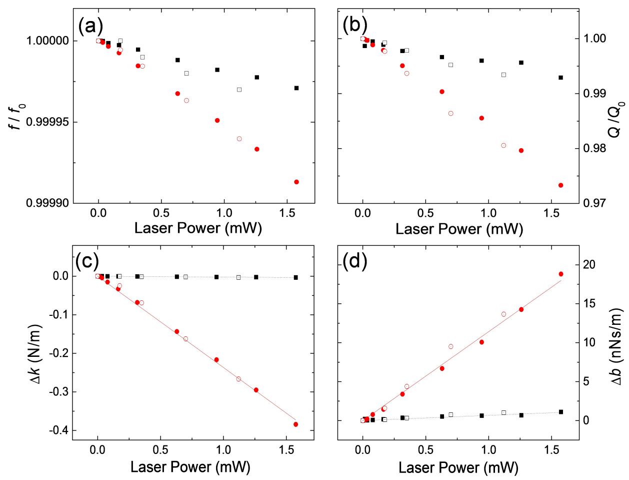

FIG. 5. (a) Relative resonance frequency and (b) relative quality factor as a function of average laser power at the tip apex. f_0 and Q_0 are the values obtained in the absence of laser light. (c) Extracted change in the cantilever's spring constant and (d) extracted change in the damping coefficient. First eigen mode is indicated by black squares and second eigen mode by red circles. Solid symbols denote CW irradiation and open symbols indicate illumination with pulsed laser light. Solid lines represent linear fits to the combined data (cw and pulsed) for each eigen mode.

A good estimate of the tip temperature under the different illumination conditions can be obtained by relating the resonance frequency shift data shown in Figure 5(a) with the simulations presented in Figure 2. The resulting change in temperature of the tip as a function of average laser power is shown in Figure 6 for both eigen modes and both illumination modes. It can be seen that the temperature rise of the tip is nearly invariant for both illumination conditions. In addition, the estimated temperature rise is virtually the same whether determined through the dynamics of the first or the second eigen mode, as required. The similarity in the temperature rise determined from different data sets fosters confidence in the method pursued, and that the extracted change in temperature represents a meaningful estimate of the actual temperature. Based on our analysis, the temperature rise of the tip is $\sim$ 7.5 K/mW for the gold-coated tip used here and with 532 nm laser radiation.

V. PHOTO-INDUCED FORCE MICROSCOPY

Having established the response of the retracted tip/cantilever system to laser heating at the tip, we next

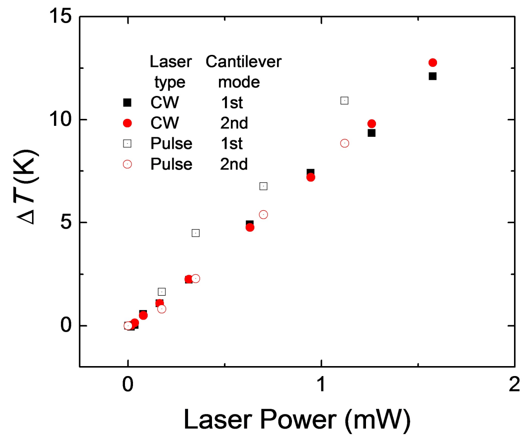

FIG. 6. Estimated temperature rise ΔT as a function of the incident average laser power. The temperature rise is obtained by relating the measured changes in f/f_0 to the corresponding simulation results.

examine the effects of the applied thermal load on the PiFM signal under ambient conditions. A schematic of the PiFM setup can be found in Ref.[5,22]. Our goal is to determine whether laser heating introduces a significant artifact or whether the effects are too small to affect the measurements in a significant manner.

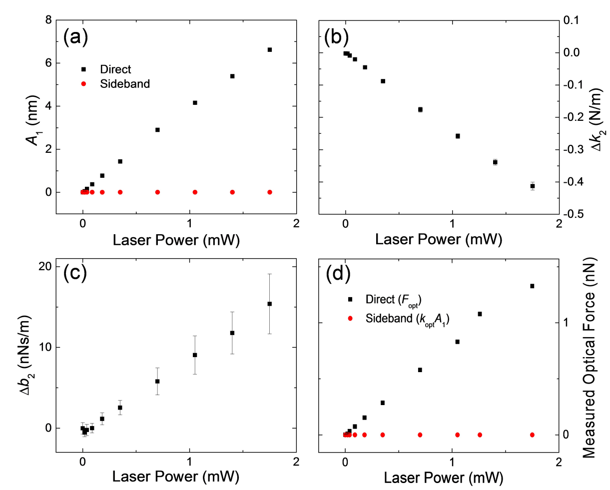

FIG. 7. (a) Oscillation amplitude A_1 as a function of average laser power as measured in PiFM. Each data point is the average value of various measurements in the range from 30 to 150 nm for the tip/sample. (b) Change in the spring constant Δk_2 obtained by measuring A_2 and θ_2 during the PiFM measurement. (c) Change in the damping coefficient Δb_2. (d) Retrieved photo-induced force.

Figure 7(a) shows the measured oscillation amplitude A_1 in the PiFM channel, both for direct (black) and sideband (red) detection, as the laser power on the tip is increased. Amplitude measurements are performed with the tip retracted to a distance of 30-150 nm from the glass coverslip surface, at 5 nm intervals of the tip-sample distance. We find that within this range the oscillation amplitude is insensitive to tip-sample distance. This indicates that the exerted force does not sample the effect of the glass surface and that the spatial profile of the focused light field is nearly constant within this range. The measured A_1 shown in Figure 7(a) is the average of the measurements performed in the 30-150 nm range. It is seen that the amplitude in the direct detection mode increases linearly with laser power, whereas the amplitude in the sideband detection mode is near the noise floor for all measurements. The negligible signal in the sideband mode indicates that the gradient of the force is very small. This is expected, as far from the glass surface the F_{int} can be ignored and no significant z-dependence of the force is anticipated. The linear increase measured in the direct mode follows the expected trend of the scattering force F_{scat}, which depends linearly on the light intensity.

Along with the A_1 measurements, amplitude and phase variations in the A_2 channel are simultaneously recorded. With the driving force F_d known, we may use Eqs. (10) and (11) to compute the intensity dependent Δk_2 and Δb_2. The results are shown in Figures 7(b) and (c). Similar to the results presented in Figures 5(c) and (d), which are obtained through direct resonance frequency shift measurements, we find that the spring constant decreases linearly with laser power and the damping coefficient increases linearly with laser power. Note that the method of obtaining these values is rather different in Fig. 5 compared to Fig. 7, yet the retrieved Δk_2 and Δb_2 from these measurements are identical to within experimental uncertainty. This observation fosters confidence that the amplitude and phase measurements in the A_1 and A_2 channels of the PiFM measurement are sufficient for retrieving information about the temperature dependent changes to the cantilever resonance.

Using the α and β values obtained in Section IV, we can now calculate the photo-induced force from Eq. 12. Figure 7(d) shows the retrieved force measured in the direct (black) and sideband (red) modes. We see that the absence of a strong spatial dependence of the force, and thus the gradient of the force, suppresses the signal in the sideband mode. In the direct mode, we observe a linear increase of the force with laser power, indicative of F_{scat}. This suggests that the PiFM measurement is dominated by the scattering force. The question arises to what extent the measurement is affected by the heat induced changes to the cantilever's mechanical resonance.

To address this question, we plot the individual contributions of Eq. 12 in Fig. 8. The total photo-induced force, reproduced from Fig. 7(d), is indicated by the open circles. The scattering force F_{scat}, obtained as the first term of Eq. 12, is shown as blue triangles. This contribution changes linearly with the laser power, as is evident from the linear fit shown in the graph. The laser power dependence of the second term of Eq. 12, symbolized as F_{heat}, is plotted as red squares. A fit reveals that this contribution scales quadractically with the laser power. This dependence can be rationalized by the fact that both A_1 as well as Δk_1 and Δb_1 depend linearly on the intensity of the applied laser beam. Since F_{heat} relies on the product of A_1 with either Δk_1 or Δb_1, the resulting laser power dependence is quadratic. However, F_{heat} is more than one order of magnitude smaller than F_{scat} over the entire range of examined laser powers, suggesting that its effect is minimal under typical experimental conditions. Finally, the cross term in Eq. 12 is found to be negligibly small under all conditions, due in part to the difference in sign between Δk_1 and Δb_1, which causes their respective terms to counteract. Therefore, the current analysis reveals that F_{opt} is dominated by F_{scat} and that the effects of heating-induced changes to the cantilever's resonance are at least an order of magnitude smaller under experimentally relevant conditions.

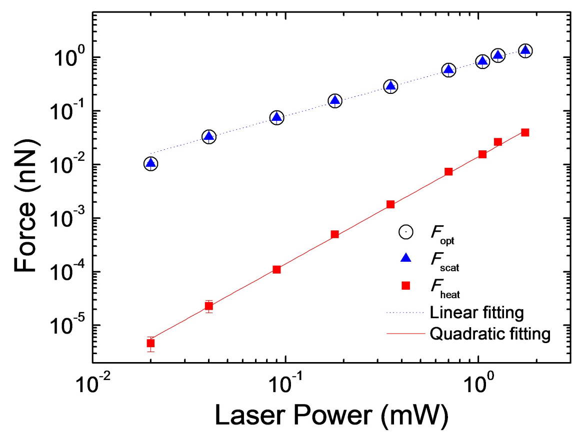

FIG. 8. Decomposition of the measured force F_{opt} (open circles) into the scattering force F_{scat} (blue triangles) and an effective force F_{heat} due to laser heating (red squares). F_{scat} increases linearly with laser power while F_{heat} shows a quadratic dependence.

VI. DISCUSSION

In this work, we have carefully examined the effects of laser-induced heating of the tip on the cantilever's mechanical properties, along with its implications for PiFM measurements. We have focused explicitly on the limit of large tip-sample distances, a situation in which tip-sample interactions can be ignored. In this limit, heating related changes to the mechanical properties of the cantilever, as a consequence of coupling light to its atomically sharp tip, can be examined in detail.

The resonance curve shift measurements provide clear evidence that under experimentally relevant conditions the thermal load applied through laser illumination affects the resonance frequency of the cantilever. We find that the resulting temperature gradient in the cantilever body effectively softens the beam and thus decreases the frequency as well as the quality factor of the mechanical resonance. We observe similar trends for the first and second mechanical resonances of the cantilever, although the effects for the second resonance are more pronounced. For the gold-coated cantilever examined, we find a frequency shift of $\sim$ 30 Hz for the first mode and a frequency shift of $\sim$ 0.83 kHz for the second mode when the λ = 532 nm laser power is raised to 1.5 mW. At the same time, the Q-factor for the first mode decreases by 1%, whereas the Q-factor for the second resonance is reduced by as much as 3%.

The observed effects do not appear to depend on whether the laser is operating in cw or pulsed mode. This indicates that the measured heating effect is linear and thus independent of the peak intensity of the laser pulses. Using FEM simulations of a cantilever with identical dimensions as used in the experiments, we have obtained quantitative insight in how the temperature rise at the tip produces a shift in the resonance frequency of the cantilever. By relating the simulations to the resonance curve shift measurements, we have found that the temperature increase (ΔT) at the tip amounts to $\sim$ 7.5 K/mW of laser power. This result is remarkably consistent among both cw and pulsed measurements and independent of whether the heating effect is examined through the first or second resonance of the cantilever. The temperature increase of the tip found here is higher than reported previously for a silicon tip irradiated with a 800 nm fs laser beam, which yielded a ΔT of $\sim$ 1.3 K/mW over a range of 0-50 mW average laser power[18]. This difference can be attributed to the different tip geometry, the presence of a gold coating in our measurements, and the different wavelength used.

The applied average power in laser-based scan probe measurements, including PiFM, typically ranges from 10 μW to several mW. Although the use of gold-coated tips enhances the optical response of the tip's apex, the presence of plasmonic resonances also increases the amount of energy absorbed by the material from the light field. In the present study, we have used a gold-coated tip coupled to 532 nm light. The excitation wavelength is close to the plasma frequency of gold, and appreciable absorption of light can be expected under these conditions. The determined temperature rise of $\sim$ 7.5 K/mW of laser power is significant, and cannot be simply ignored in scan probe measurements without further examination.

We have studied the effect of heating-induced mechanical changes on PiFM measurements in the limit of the retracted tip. The main observation is that the measured $F_{\rm opt}$ is dominated by $F_{\rm scat}$ and that the effects of heating are at least an order of magnitude lower. This implies that under experimental conditions relevant to PiFM, heating of the tip and the subsequent changes to the mechanical resonance do not impose a significant perturbation to the accuracy of $F_{\rm scat}$ measurements.

Although these results serve as a helpful reference when performing PiFM measurements, the current study does not rule out a negative impact from heating-related artifacts. First, since the heating-induced contribution $F_{\rm heat}$ changes quadratically with laser power relative to the linear dependence of $F_{\rm scat}$, the effects of laser heating grow more significant at higher laser powers. Second, these results pertain to the limit of large tip-sample distances, whereas PiFM measurements are commonly performed to examine forces when the tip is in close proximity with the sample. The electromagnetic forces between the induced dipoles in the tip and the sample are generally orders of magnitude weaker than the $F_{\rm scat}$ forces studied here, making them more vulnerable to heating-induced changes of the cantilever resonances. In addition, in the tapping mode and in the full contact regime, forces related to thermal expansion of the sample can be substantial and come to dominate the PiFM measurement[16].

VII. CONCLUSION

This work provides insight into one of the mechanisms by which heating can affect laser-based scan probe measurements. Illumination of cantilevered tips by tightly focused laser beams gives rise to a temperature increase of the cantilever/tip system. The experiments and simulations in this work provide evidence that tip heating leads to a temperature gradient in the cantilever body, which effectively softens the beam, thereby decreasing the frequency and quality factor of the mechanical resonance. Using gold-coated tips and a laser wavelength of 532 nm, changes in the resonance frequency amount to 10^{-2}% when the average laser power is raised to 1.5 mW, whereas the Q-factor changes as much as 3% under these conditions. Comparison between experiments and simulations reveals a temperature increase of $\sim$ 7.5 K/mW of laser power at the tip. Despite the heating-induced changes to the cantilever's mechanical resonance, the PiFM signal remains relatively unaffected and accurate measurements of the scattering force can be performed, at least in the limit of large tip-sample distances.

ACKNOWLEDGMENTS

This work was supported by Chemistry at the Space-Time Limit (CaSTL), a Center for Chemical Innovation sponsored by the National Science Foundation, grant CHE-1414466.

* Correspondence: epotma@uci.edu

1. J. Jahng, F. T. Ladani, R. M. Khan, X. Li, E. S. Lee, and E. O. Potma, Opt. Lett. **40**, 5058 (2015).
2. T. Tumkur, X. Yang, C. Zhang, J. Yang, Y. Zhang, G. V. Naik, P. Nordlander, and N. J. Halas, Nano letters **18**, 2040 (2018).
3. M. Tamagnone, A. Ambrosio, K. Chaudhary, L. A. Jauregui, P. Kim, W. L. Wilson, and F. Capasso, Science Advances **4** (2018), 10.1126/sciadv.aat7189.
4. J. Liu, S. Park, D. Nowak, M. Tian, Y. Wu, H. Long, K. Wang, B. Wang, and P. Lu, Laser & Photonics Reviews **12**, 1800040 (2018).
5. J. Jahng, J. Brocious, D. A. Fishman, F. Huang, X. Li, V. A. Tamma, H. K. Wickramasinghe, and E. O. Potma, Physical Review B **90**, 155417 (2014).
6. I. Rajapaksa, K. Uenal, and H. K. Wickramasinghe, Applied physics letters **97**, 073121 (2010).
7. J. Jahng, D. A. Fishman, S. Park, D. B. Nowak, W. A. Morrison, H. K. Wickramasinghe, and E. O. Potma, Accounts of chemical research **48**, 2671 (2015).
8. D. Nowak, W. Morrison, H. K. Wickramasinghe, J. Jahng, E. Potma, L. Wan, R. Ruiz, T. R. Albrecht, K. Schmidt, J. Frommer, D. P. Sanders, and S. Park, Science Advances **2** (2016), 10.1126/sciadv.1501571.
9. J. Jahng, J. Brocious, D. A. Fishman, S. Yampolsky, D. Nowak, F. Huang, V. A. Apkarian, H. K. Wickramasinghe, and E. O. Potma, Applied Physics Letters **106**, 083113 (2015).
10. I. Rajapaksa and H. Kumar Wickramasinghe, Applied Physics Letters **99**, 161103 (2011).
11. H. U. Yang and M. B. Raschke, New Journal of Physics **18**, 053042 (2016).
12. B. T. OCallahan, J. Yan, F. Menges, E. A. Muller, and M. B. Raschke, Nano Letters **18**, 5499 (2018).
13. A. M. Katzenmeyer, V. Aksyuk, and A. Centrone, Analytical Chemistry **85**, 1972 (2013).
14. A. Dazzi and C. B. Prater, Chemical Reviews **117**, 5146 (2017).
15. L. Wang, H. Wang, M. Wagner, Y. Yan, D. S. Jakob, and X. G. Xu, Science Advances **3** (2017), 10.1126/sciadv.1700255.
16. J. Jahng, E. O. Potma, and E. S. Lee, Analytical Chemistry **90**, 11054 (2018).
17. B. T. OCallahan and M. B. Raschke, APL Photonics **2**, 021301 (2017).
18. A. A. Milner, K. Zhang, V. Garmider, and Y. Prior, Applied Physics A **99**, 1 (2010).
19. L. Xu, F. Qian, and Y. Liu, AIP Advances **5**, 117116 (2015).
20. B. Kim, Q. H. Kim, S. Kwon, S. An, K. Lee, M. Lee, and W. Jhe, Phys. Rev. Lett. **111**, 246102 (2013).
21. J. Jahng, F. T. Ladani, R. M. Khan, and E. O. Potma, in *Complex Light and Optical Forces X*, Vol. 9764 (International Society for Optics and Photonics, 2016) p. 97641J.
22. J. Jahng, B. Kim, E. S. Lee, and E. O. Potma, Physical Review B **94**, 195407 (2016).
23. J. Yamanishi, Y. Naitoh, Y. J. Li, and Y. Sugawara, Applied Physics Letters **110**, 123102 (2017).
24. R. K. Endo, Y. Fujihara, and M. Susa, High Temp.-High Pressures **35**, 505 (2003).
25. W. C. Ang, P. Kropelnicki, O. Soe, J. H. Ling, A. Randles, A. Hum, J. Tsai, A. A. Tay, K. Leong, and C. S. Tan, Journal of Micromechanics and Microengineering **22**, 085015 (2012).
26. Y. Okada and Y. Tokumaru, Journal of applied physics **56**, 314 (1984).
27. J. Dolbow and M. Gosz, Mechanics of Materials **23**, 311 (1996).
28. C.-H. Cho, H.-Y. Cha, and H.-K. Sung, Journal of Semiconductor Technology and Science **16**, 153 (2016).
29. J. Broekmaat, A. Brinkman, D. H. Blank, and G. Rijnders, Applied physics letters **92**, 043102 (2008).
30. F. Aguilar Sandoval, M. Geitner, É. Bertin, and L. Bellon, Journal of Applied Physics **117**, 234503 (2015).
31. U. Gysin, S. Rast, P. Ruff, E. Meyer, D. W. Lee, P. Vettiger, and C. Gerber, Physical review B **69**, 045403 (2004).
32. K. Kunal and N. R. Aluru, Physical Review B **84**, 245450 (2011).
33. J. Rodriguez, S. A. Chandorkar, C. A. Watson, G. M. Glaze, C. Ahn, E. J. Ng, Y. Yang, and T. W. Kenny, Scientific reports **9**, 2244 (2019).